# Numerical Study of a Centrifugal Platform for the Inertial Separation of Circulating Tumor Cells Using Contraction-Expansion Array Microchannels

## Ebrahimi, Sh[1, 2], Tahmasebipour, M[1, 2] *

*1. Faculty of New Sciences and Technologies, University of Tehran, Tehran, 14395 -1561, Iran*
*2. Micro/Nanofabrication Technologies Lab, Faculty of New Sciences and Technologies, University of Tehran, Tehran, 14395 -1561, Iran*

## Abstract

Label-free inertial separation of the circulating tumor cells (CTCs) has attracted significant attention recently. The present study proposed a centrifugal platform for the inertial separation of the CTCs from the white blood cells. Particle trajectories of the contraction-expansion array (CEA) microchannels were analyzed by the finite element method. Four expansion geometries (i.e., circular, rectangular, trapezoidal, and triangular) were compared to explore their differences in separation possibilities. Different operational and geometrical parameters were investigated to achieve maximum separation efficiency. Results indicated that the trapezoidal CEA microchannel with ten expansions and a 100 µm channel depth had the best separation performance at an angular velocity of 100 rad/s. Reynolds number of 47 was set as the optimum value to apply minimum shear stress on the CTCs leading to 100% efficiency and 95% purity. Furthermore, the proposed system was simulated for whole blood by considering the red blood cells.

**Keywords:** CEA microchannel, Centrifugal microfluidic system, Lab-on-a-disk, Inertial microfluidic, Numerical simulation

## 1. Introduction

According to the American Cancer Society reports for 2025, 16 million people will be diagnosed with cancer (1). Circulating tumor cells (CTCs) are the main markers in the primary detection of cancer metastasis, analyses of cancer progression, and exploration of suitable treatment techniques. The CTCs dissociate from the initial tumor, travel through the bloodstream to another organ, and form new tumors (2). As reported by the World Health Organization, 30% of cancer deaths can be prevented with early diagnosis. Therefore, the separation and analysis of CTCs is a crucial step in cancer treatment (3, 4). Microelectromechanical sensors (5, 6) and actuators (7,

8) are suitable in the biomedical field for different applications (9). Microfluidic, as a part of microelectromechanical systems (MEMS), is extensively utilized in point-of-care (POC) cell separation devices owing to its desirable properties, such as low required sample amount, excellent sensitivity, and portability (10).

Since CTCs are rare, isolating these cells requires accurate and efficient systems, with high purity and throughput, and minimum damage to the cell (11). Lab-on-chip systems (LOC) allow the separation of these rare particles based on their size in both active and passive methods (12). Since active processes take advantage of external forces, their complexity

and difficult integration into microfluidic systems make them an incompatible choice for LOD tests. However, passive methods of particle separation rely on microchannel geometry and hydrodynamic forces (13). Among the various passive methods, inertial microfluidic is one of the most considered methods for separating CTCs because of its substantial features, including high throughput, simple structure, label-free, and low cost. Compared to the other size-based separation approaches, inertial microfluidics has low purity considering the size overlapping of the CTCs and the other cells; however, designing different channel geometries (14, 15) with specific dimensions can achieve high purity in this technique for CTC separation. In inertial focusing, suspended particles within a fluid travel through fluid flow and can be ordered in specific positions. This behavior occurs because of inertial Lift ($F_L$) and Dean Drag ($F_D$) forces in the channel and can be determined via channel shape and fluid properties (16). Similar to the curved shape channels, because of the abrupt change of the cross-section in the contraction-expansion arrays (CEAs) channel, fluid streamlines are curved when they get in the expansion zone, producing two vortexes at the bottom and top of the channel cross-section area, which is well-known as Dean flow. Lee, Park (17) proposed asymmetric contraction expansion arrays to isolate MCF7 from blood components. Their experimental work achieved a recovery rate of 99.1% with a throughput of $1.1 \times 10^{8}$ cell/min. Che, Yu (18) used a CEA microchannel to isolate CTCs with efficiency.

Centrifugal platforms, also called lab-on-disk (LOD), are novel technologies in microfluidics, in which microchips are designed on a disk. In these platforms, the fluid is driven by the intrinsic forces of the rotating disk and simplifies these systems due to the lack of need for external connections and pumps (19). Lab-on-disk has extensively been studied for the separation of

blood components, such as plasma (20), separation of CTC by functionalizing these cells with magnetic microbeads (21), and fluid mixing (22). An LOD device provides some attractive advantages for particle separation, such as an inexpensive setup, the ability to integrate multiple operating units, and process automation. The use of size-based inertial particle separation in LOD systems is an efficient and label-free method. Morijiri, Sunahiro (23) developed a cell separation method called pinched flow fractionation in a centrifugal platform for separating stand on density and particle size. Maria, Gerson (24) designed spiral asymmetric channels to study the focusing of particles in a system for the separation of silica and polystyrene particles with the same size (21) and two different densities with high efficiencies. In another study (25), the researchers used the same channel design for circulating tumor cells (MCF7s) focusing on a LOD system. It was found that compared to LOC systems, in LOD devices, particle focusing occurs at low Reynolds numbers due to the centrifugal ($F_C$) and Coriolis ($F_{Cor}$) forces. Shamloo and Mashhadian (26) examined the focusing behavior of polystyrene particles in a serpentine microchannel on a centrifugal platform.

The CEA channel employs inertial forces in fixed directions and magnitudes to separate and focus particles. Recently, Al-Halhouli, Doofesh (27) conducted contraction-expansion arrays for particle focusing in a LOD system with trapezoidal chambers. Nasiri, Shamloo (28) considered square-shaped expansions to separate CTCs from white blood cells (WBCs). They observed a separation efficiency of at an angular velocity of 2,000 RPM ($\omega = 204.9$ rad/s). Table 1 outlines the major characteristics of particle separation and focusing by integrating passive inertial microfluidic in the LOD systems. To the best of our knowledge, few studies have been published on integrating the inertial separation unit in the centrifugal platform, despite its numerous advantages and a high potential for POC devices.

**Table 1.** Main characteristics of the reported in LOD systems for the particle/cell inertial separation/focusing

| Geometry | Cross-section | Width (μm) | Height (μm) | Micro-particles and their sizes | Distance from disk center | Rotational speed or frequency of disk | Separation efficiency | Ref |
|---|---|---|---|---|---|---|---|---|
| Serpentine channel with three corner angels (90°, 85°, 75°) | Rectangular | 200 | 40 | PS: 8 μm, 9.9 μm and 13 μm | 3 cm | 240 rad/s-500 rad/s | Best focusing performance for 90° | (26) |
| Pinch flow fractionation and curved channel with 12 outlets | Rectangular | 350 | 10 | Fluorescent PS: 3 μm and 5 μm Silica microbeads with 5 μm | 15 mm | 750 RPM | 98% silica at outlet 5 86% 3 μm PS at outlets 10, 11, and 12 | (23) |
| Square contraction-expansion arrays | Square | 100 | 100 | WBC: 10 μm CTC: 20 μm | 3 cm | 2000 RPM | 90% separation | (28) |
| Trapezoidal contraction-expansion arrays | Rectangular | 120 | 50 | PS: 5 μm and 10 μm | 8 mm | 2000 RPM | 98.7% focusing of 10 μm 93.75% focusing for 5 μm | (27) |
| Asymmetric serpentine with small and large curves | Rectangular | 350 and 650 | 72 | Functionalized MCF7 (breast cancer cells) and PS beads | 12 mm | 3.75 Hz | 92.5% focusing at Reynolds number of 11 | (25) |
| Asymmetric serpentine curved channel with a 6-8 turn | Rectangular | 350-650 | 72 | PS and silica: 21 μm | N/A | 3.75-6.25-8.75 Hz | High separation at 3.75 Hz | (24) |

PS: Polystyrene; WBC: White blood cell; CTC: Circulating tumor cell

outlines the major characteristics of particle separation and focusing by integrating passive inertial microfluidic in the LOD systems. To the best of our knowledge, few studies have been published on integrating the inertial separation unit in the centrifugal platform, despite its numerous advantages and a high potential for POC devices.

Investigation of a device using numerical simulation is necessary to reduce the fabrication cost and experimental errors (29). In LOD systems, simulation is an excellent guide for researchers to analyze particle behavior (30). The present study aimed to utilize two cell isolation techniques to find out an ideal POC device that could enjoy the advantages of both inertial

and centrifugal microfluidics. In this research, the separation characteristics of different CEA channel geometries were investigated using numerical simulations. Particle trajectories were obtained for different expansion arrays, and separation parameters were compared. For the best channel geometry, various parameters were evaluated to determine the desirable separation conditions.

Figure 1 shows an illustration of the separation mechanism in the proposed system. Blood is injected into the inlet chamber without the need for a pump. The system starts to rotate higher than the disk burst frequency, and after that the separation is completed, the samples are collected from the designed outlets.
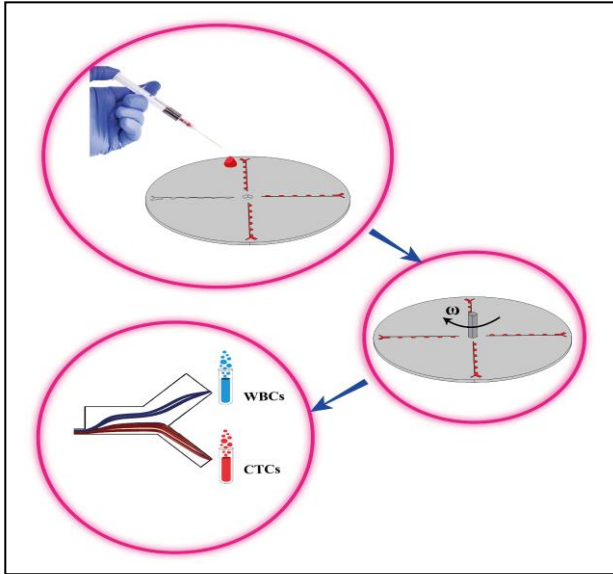
**Figure 1**. Graphical abstract

## 2. Materials and Methods

### 2.1. Microchannel Geometry

The present study investigated the inertial separation of CTCs from WBCs in four CEA microchannel geometries integrated into an LOD system. Figure 2 shows the schematic of the trapezoidal arrays microchannel. The simple-structure microchannel has 21.55 mm length with a square cross-section and consists of 1 inlet and 2 outlets. The microchannel is located at a 3-cm distance from the disk's center. Incubated blood containing WBC and CTCs enters the microchannel without the need for a pump. Table 2 presents the geometrical parameters for four microchannel types. As depicted in figure 3, the microchannel unit has a 900 µm length.
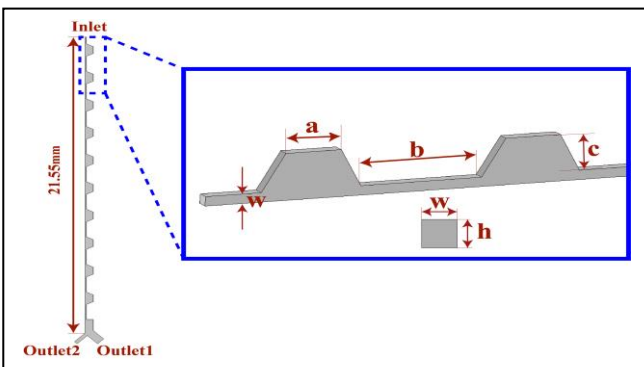


**Figure 2**. Illustration of the separation microchannel with designed parameres

**Table 2**. Microchannel dimensions for four expansion geometries

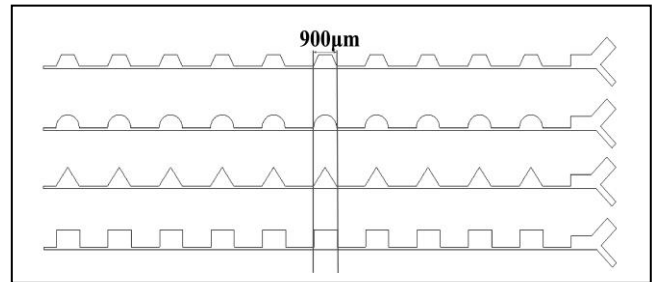| Parameter (µm) | a | b | c | w | h |
|---|---|---|---|---|---|
| **Trapezoidal** | 500 | 1100 | 500 | 100 | 100 |
| **Circular** | - | 1100 | 450 | 100 | 100 |
| **Triangular** | - | 1100 | 650 | 100 | 100 |
| **Rectangular** | 900 | 1100 | 600 | 100 | 100 |



**Figure 3**. Top view of the four contraction-expansion array micro-channels

### 2.2. Governing Equations

In LOD systems, the Centrifugal ($F_C$) and Coriolis ($F_{Cor}$) forces drive the fluid in a rotating disk (31). On a rotating platform with a velocity of ω, the $F_C$ and $F_{Cor}$ can be written as follows:

$$F_C = \rho_f r \omega^2 \quad (1)$$

$$F_{Cor} = 2\rho_f \omega U \quad (2)$$

Where, $\rho_f$ is a volume density for a fluid, r is a radial location, and U is the fluid's velocity. There is an Eulerian force in centrifugal platforms due to the change in angular velocity. Since in the present study ω is constant then amount of the Eulerian force is 0. Equations (1) and (2) in the Cartesian coordinates are expressed as follows (24):

$$f_x = \rho_f \omega^2 x + 2\rho_f \omega \upsilon \quad (3)$$

$$f_y = \rho_f \omega^2 y - 2\rho_f \omega u \quad (4)$$

$$f_z = 0 \quad (5)$$

Where *v* and *u* are the fluid velocities in the y and x directions, respectively.

Despite the non-Newtonian behavior of the whole blood in the experimental separation of CTCs, these

cells are mixed with diluted whole blood. Therefore, in numerical simulations, the use of a Newtonian fluid with water properties is acceptable. Governing equations for laminar Newtonian and incompressible fluid flow are the continuity Equation (Equation 6) for mass conservation and Navier-Stokes (Equation 7) Equations for momentum conservation (16):

$$\nabla \cdot (\rho_f \vec{U}) = 0 \tag{6}$$

$$\rho_f \frac{\partial \vec{u}}{\partial t} + \rho_f (\vec{U} \cdot \nabla \vec{U}) = -\nabla P + \mu \nabla^2 \vec{U} + \vec{f_b} \tag{7}$$

Where $\vec{U}$ is the fluid velocity vector (m/s), P is the pressure (Pa), μ is the dynamic viscosity (N.s/m²), and $\vec{f_b}$ is the sum of all body forces (N.s/m³), which for a LOD system includes $F_C$ and $F_{Cor}$:

$$\vec{f_b} = \vec{F_C} + \vec{F_{Cor}} \tag{8}$$

In a LOD system, $F_C$ and $F_{Cor}$ are also felt by the suspended particles in the fluid. In this case, the Equations of centrifugal force (1) and Coriolis force (2) for spherical particles with density, diameter, and velocity of $\rho_p$, a, and $U_p$ respectively, are expressed as following (28):

$$F_C = \frac{\pi a^3 (\rho_p - \rho_f)}{6} r \omega^3 \tag{9}$$

$$F_{Cor} = \frac{\pi a^3 (\rho_p - \rho_f)}{6} U_p \omega \tag{10}$$

Where the subscripts p and f stand for particle and fluid, respectively.

Besides the centrifugal platform forces, particles feel $F_L$ and $F_D$ in different directions and amounts, relying on the velocity profile, particle size, fluid features, and channel dimensions. In this microfluidic device, the applied $F_L$ on the particles, which is the balance between shear-gradient and wall-induced $F_L$, can be expressed as follows (32):

$$F_L = C_L \frac{\rho_f U_{max}^2 a^4}{D_h^2} \tag{11}$$

Where $U_{max}$ is the maximum fluid velocity, $a$ is the particle diameter, and $D_h$ denotes the hydrodynamic diameter of the channel defined as a , where w and h are the width and height of the micro-channel cross-section, respectively. $C_L$ is the dimensionless coefficient of lift force, which is related to the particle location across the channel cross-section while assuming an average value of 0.5 for rectangular cross-section. The channel Reynolds number represents the ratio of inertial forces over viscous forces. It is defined as (33):

$$Re_c = \frac{\rho_f U_{max} D_h}{\mu} \tag{12}$$

Similar to the curved shape channels, because of the abrupt change of the cross-section in the CEA channels, fluid streamlines are curved when they get in the expansion zone, producing Dean Vortices at the bottom and top of the channel cross-section area. Using the Stokes drag equation, the applied $F_D$ on the particles can be calculated as the following:

$$F_D = 3 \pi \mu U_D a \tag{13}$$

Where $U_D$ is the mean velocity of the Dean flow for a channel with $Re_c$ and a radius of curvature R and can be determined as follows:

$$U_D = 1.8 \times 10^{-4} De^{1.63} \tag{14}$$

$$F_D = 5.4 \times 10^{-4} \pi \mu De^{1.63} a \tag{15}$$

The dimensionless number $De = Re_c \sqrt{\frac{D_h}{2R}}$ indicates the magnitude of the Dean flow.

To determine the motion of the particles, Newton's law of motion is solved (34):

$$m_p \frac{d^2 \vec{r_p}}{dt^2} = \vec{F_D} + \vec{F_L} + \vec{F_C} + \vec{F_{Cor}} \tag{16}$$

Where $m_p$ is the particle mass and $\vec{r_p}$ is a radial location vector.

## 2.3. Numerical Simulation

The COMSOL Multiphysics 5.5 software was utilized to perform the 3-dimensional simulations, and the Finite Element Method was employed to solve the Navier-Stokes equations. Table 3 summarizes the boundary conditions applied in the simulations. In laminar flow, $F_C$ and $F_{Cor}$ are applied as body forces for fluid driving based on the platform's clockwise rotation, which is added to the Navier-Stokes equations as a volume force. The velocity fields resulted from the fluid flow analysis were used as the input velocity in particle tracing. The time-dependent study approach with a time step of 0.00001s was executed with an Eulerian method. In particle tracing, the dominant forces, including $F_D$, $F_L$, and $F_C$ and $F_{Cor}$, were added to the particles. The $\rho_f$ and $\mu$ were considered to be 1,000 kg/m$^3$ and 0.001 Pa.s, respectively. The simulation was performed for the incubated blood of lung cancer, stage-IV patient, with Lysis buffer (removed red blood cells [RBCs]). For the simulations, 60 particles, including 30 CTCs and 30 WBCs (which were placed randomly in the inlet), were used with a $\rho_p$ of 1,050 kg/m$^3$ and an average diameter of 20 µm and 10 µm based on an experimental study by Zhou, Kulasinghe (35). Since the blood samples are diluted in the blood cell separation experimental works (36), particle-particle interactions were neglected in these simulations. In addition to having convenient boundary conditions and performing a properly structured mesh, particles with different sizes are sorted based on the applied forces into two various outlets. In the introduced microchannel, particles' lateral migration strongly depends on the particle size; therefore, label-free separation of the CTCs from white blood cells is possible.

**Table 3.** Boundary conditions used in the performed simulations

| Physics | Inlet | Walls | Outlet |
|---|---|---|---|
| Laminar Flow (spf) | Normal flow P0=0 | No-slip | Suppress backflow P0=0 |
| Particle tracing (fpt) | Velocity field (spf) | Bounce | - |

## 3. Results and Discussion

### 3.1. Validation

To validate the simulations, our numerical method was used to simulate the experimental work reported for the inertial particle focusing on a LOD system Al-Halhouli, Doofesh (27). In this work, 10-µm polystyrene particles, after passing through the 30-mm channel, were focused and collected in outlet 1 (micro-chambers side) due to the hydrodynamic forces exerted by the trapezoidal micro-chambers. The particles' equilibrium position was shifted toward the sidewall with trapezoidal micro-chambers because the wall-induced lift force had vanished, leading the particle to move into the micro-chamber. The governing equations and boundary conditions were applied to the fluid flow and the particle tracing, and then the simulation was run. Figure 4 shows the collection of particles at the desired outlet (outlet 1).
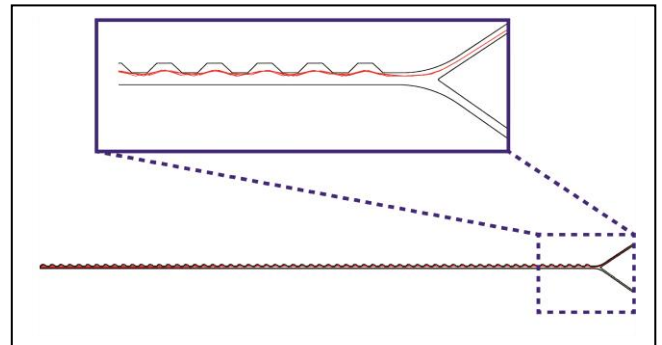


**Figure 4**. Collection of the particles in outlet 1 (Redline is particle trajectory)

### 3.2. Mesh Independency

A structured uniform mesh was used to discretize the computational domain. Subsequently, the mesh independence analysis was performed. For each channel geometry, structured meshes with an average quality of 0.93 were used. The maximum radial velocity was demonstrated in a cross-section of the contraction zone for different grid numbers. It was observed that there was a small difference in the velocity value (error=0.085%) between 2,148,500 and 2,849,854 elements. Although an increase in the mesh elements did not change the evaluated measure, it expanded the computational time. Therefore, 2,148,500

was determined as the number of necessary elements to solve the simulation (Figure 5). Figure 6 depicts the mesh quality for the trapezoidal expansion arrays.
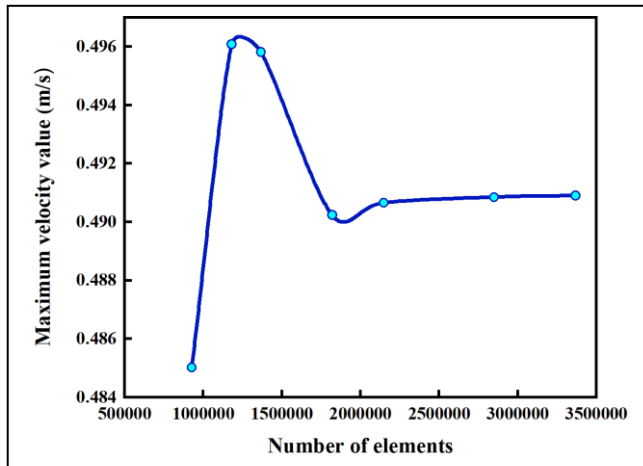


**Figure 5**. Mesh independency analysis for the maximum velocity value at different mesh elements
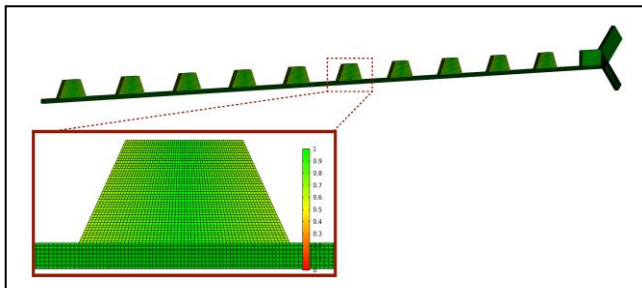


**Figure 6**. Channel mesh quality for 2,148,500 elements

### 3.3. Dean Vortex Formation

To ensure the vortex formation in four-channel types, Dean flow contours were obtained. Because of the abrupt change of the CEA microchannel cross-section, acceleration and deceleration of the flow velocity are acquired when the fluid enters the contraction and expansion zones (33). In centrifugal platforms, if Dean Vortices form in a longer part of the contraction zone of the microchannel, the Coriolis force, together with the Dean Flow, improves the secondary flow. Contraction zones with 1,200 µm lengths were considered in the present study. Figure 7 illustrates the Dean flow contours in the CEA microchannel at an angular velocity of 100 rad/s.

### 3.4. Separation Parameters

The most common parameters for evaluating separation performance are purity and separation efficiency. Purity and separation efficiency can be defined as:

$$purity = \frac{number\ of\ target\ cells\ in\ the\ target\ outlet}{total\ cells\ (WBC + CTC)\ in\ the\ target\ outlet} \times 100$$

$$separation\ efficiency = \frac{number\ of\ target\ cells\ in\ the\ target\ outlet}{total\ number\ of\ targeted\ cells\ in\ the\ inlet} \times 100$$

In simulations, it is possible to count two types of cells at the microchannel outlets and calculate separation parameters for the two different micro-channels. Figure 8 shows the comparison of two separate parameters for different expansion geometries. The contraction-expansion micro-channel provides a simple geometry for particles focusing and separation, compared to the spiral (24) and serpentine (26) micro-channels, which reduces the design and fabrication time and cost. Based on the results, the channel with trapezoidal expansions reaches 100% separation efficiency and 95% purity for CTCs, while the results are reverse for WBCs. Compared to the results of a previous study (28), which achieved 90% separation efficiency for CTCs at 2,000 RPM with the square expansion geometry, trapezoidal expansions showed 100 % efficiency at 1,000 RPM, which means lower shear stress on particles.
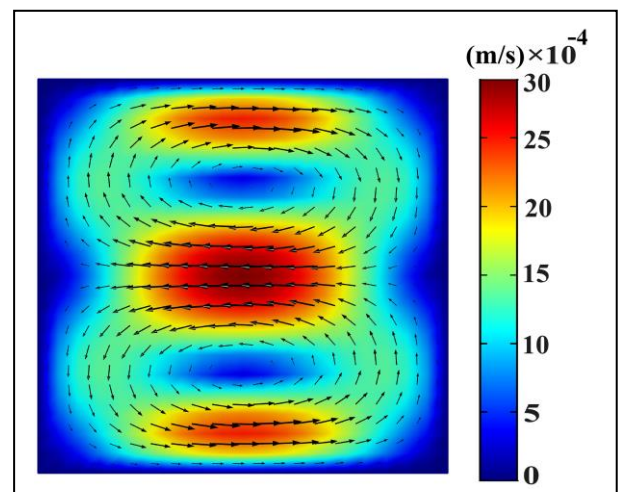


**Figure 7**. Dean Vortex formation at 30 µm of contraction region for CEA microchannel at 100 rad/s
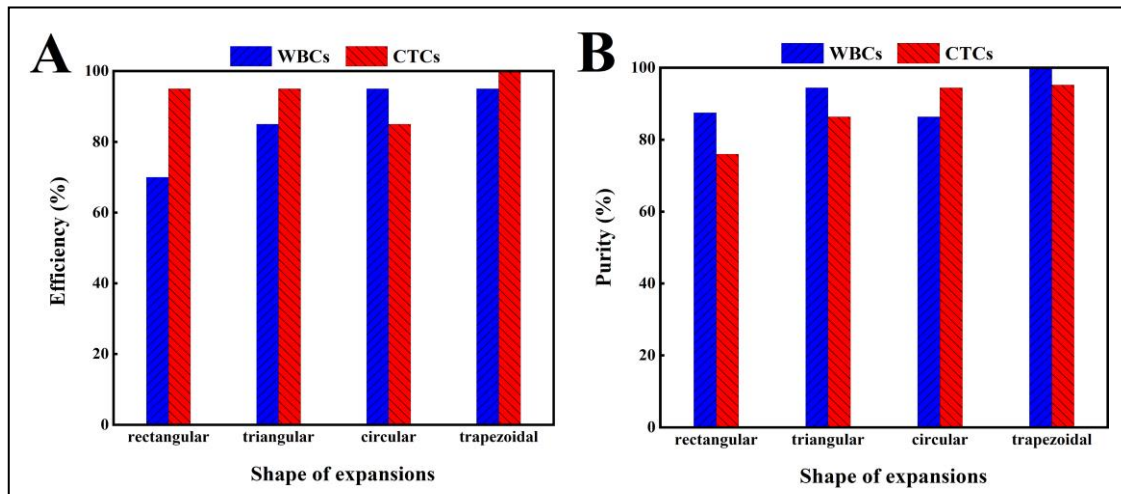
**Figure 8**. Separation efficiency and purity of WBCs and CTCs for different expansion shapes of microchannel at 100 rad/s

### 3.4.1. Effect of the Microchannel Geometry and Angular Velocity of the Disk on Particles Lateral Position

For the channel's best separation performance, lateral positions of the particles were measured near the channel outlets after ten expansions. Inertial particle separation of WBC and CTC particles was demonstrated by simulation in four microchannel types at four angular velocities. Dean flow in the contraction regions, inducing Dean Drag forces, acted on the particles depending on their size. On the other hand, since the velocity was fully developed and had a parabolic profile, particles experienced two kinds of $F_L$ (i.e., wall-induced and shear-gradient). Balancing between $F_L$ and $F_D$ determines the position of the particles. Figure 9 shows the lateral position of WBCs and CTCs for four microchannel types at different angular velocities. At high angular velocity, for all channel types, increasing the forces' acts on particles makes particles focused, decreasing the device performance. The CTCs, because of their larger size, experience greater inertial lift force than WBCs and can achieve equilibrium positions in a shorter time. As can be seen in figure 9 there was a substantial gap between the position of WBCs and CTCs in the trapezoidal expansions at 100 rad/s.

Particles experienced a smooth decrease and increase in wall-induced lift force when they entered and exited the trapezoidal expansions. Circular expansions are ideal array shapes for biological fluids, such as blood, which are likely to clog through the microchannel. Particles flow in the circular expansion microchannel more slowly, increasing the separation time. Therefore, a circular expansion microchannel is undesirable because it increases the exposure time to the particles and cell damage. The complete separation of CTCs and WBCs is obtained in triangular expansions microchannel at velocities of 150 rad/s and 200 rad/s. Moreover, based on the fluid flow analysis results, in triangular expansion arrays, the maximum velocity of the fluid is 10% more in the expansion region than in other arrays, which indicates a shorter separation time; however, high fluid velocity would make the possibility of cell damage by the high shear stress. Due to the sudden change in the wall-induced lift force, when particles enter and exit the rectangular expansions, they are arranged at wide positions, and as a result, the purity is reduced. Hence, it is concluded that when the $Re_c$ is constant, the trapezoidal CEA microchannel has advantages over the three micro-channels by the full separation of the CTC and WBC particles.
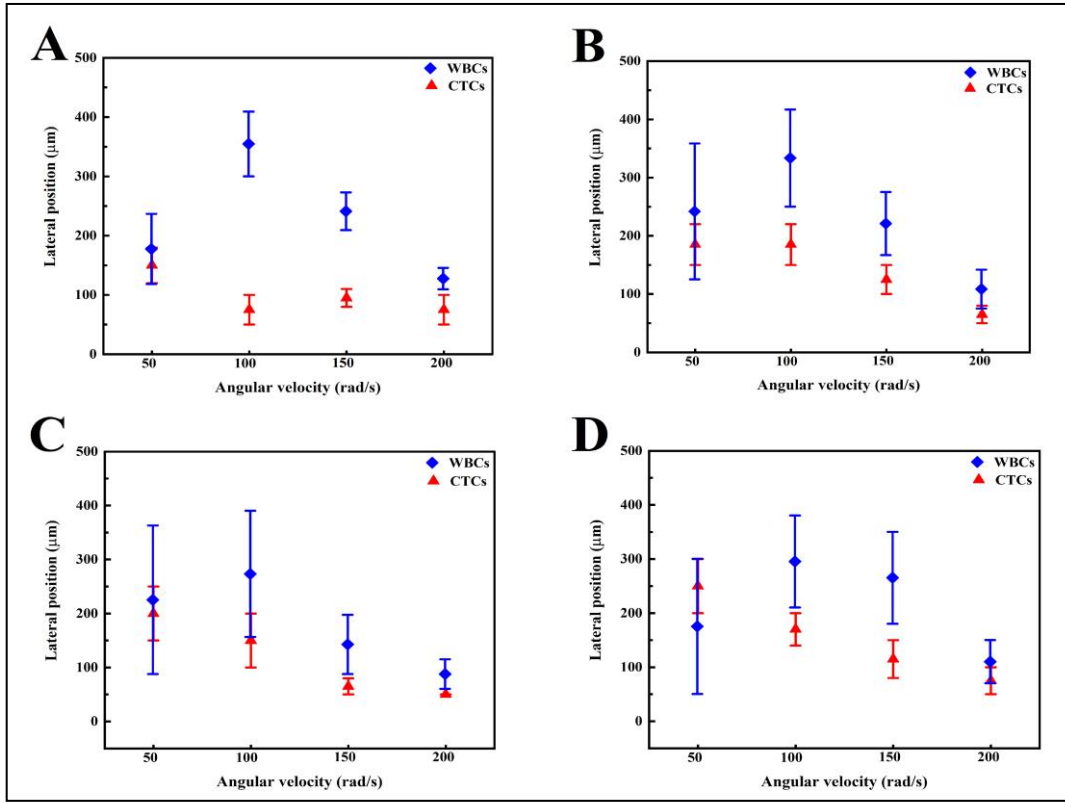
**Figure 9**. Lateral positions of the WBCs (◆ blue) and CTCs (▲ red) particles in four different micro-channels for the various angular velocities (error bars indicate the width of lateral positions); A) trapezoidal, B) circular, C) triangular, and D) rectangular expansion geometries

In the centrifugal platforms, the fluid velocity changes with the rotational velocity of the disk. Figure 10 depicts the radial velocity profiles for the different ω. To obtain the optimum ω for the disk with maximum separation efficiency, four different values of 50, 100, 150, and 200 rad/s were investigated. An increase in the $Re_c$ of the microchannel from 12.8 to 158, proportional to the rotational velocity from 50 rad/s to 200 rad/s, led to the observance of several separation patterns for the two particles' sizes. If the $Re_c$ is supposed lower than 12.8 (proportional to the ω = 50 rad/s), the $F_C$ and $F_{Cor}$ are too low, and it cannot exert the dominant $F_L$ and $F_D$ for lateral migration of the cells. Therefore, particles travel in the channel with low velocity, and the separation time increases. However, it is observed that in $Re_c$ of higher than 47 (100 rad/s), due to the enhancement of the inertial forces, separation time reduces, nevertheless, all particles share a similar path. An increase in applied

forces on the particles would possibly lead to particle damage and a reduction in particle viability at high velocities since according to Equation (11) ($F_L \propto U_{max}^2$) is directly relevant to the square of the maximum velocity along the x-axis. The best separation efficiency is obtained for the angular velocity of 100 rad/s and $Re_c$ of 47. The most crucial parameter for the CTC separation is viability; in this regard, the system should perform separation at low $Re_c$.
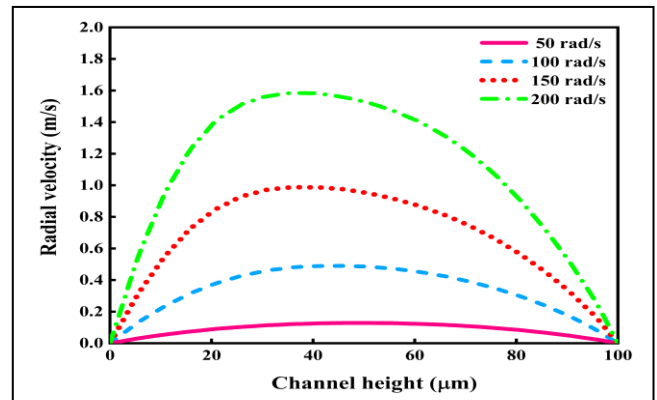


**Figure 10**. Radial velocity profiles at different angular velocities

### 3.4.2. Effect of ω on Cell Separation

The fluid flow velocity in the microchannel increases with increasing the amount of ω. Higher angular velocity results in higher forces on the cells; this makes particles be focused and collected in one outlet. On the other hand, a high angular velocity leads to a higher Reynolds number, causing a large pressure drop and possible sample leakage. Figure 11 shows the path lines of particles at different angular velocities in the trapezoidal microchannel. At trapezoidal expansions microchannel, WBC and CTC particles are affected by fully developed inertial efficacy and separated at two different angular velocities (ω =100 rad/s, and 150 rad/s). $F_C$ and $F_{Cor}$ for fluid driving and the lift and drag forces for lateral migration directly depend on the magnitude of angular velocity. At low angular velocities, such as 50 rad/s, because the radial velocity is low and the inertial effects are not enough, the particles are not separated. On the other hand, over the angular velocity of 150 rad/s, due to the enhancement of $F_L$, all particles (i.e., WBC and CTC) migrate toward outlet 2. A higher angular velocity affects particles with more shear stress, which can cause the damage and death of the biologically important particles.

### 3.4.3. Effect of the Expansion Number on Cell Separation Parameters

The difference between the particle sizes is the separation mechanism of the proposed LOD system. According to Equations 11 and 15, large particles are affected via the $F_L$, while small particles are influenced via $F_D$. It is necessary to determine the expansion numbers needed for separating CTC and WBC particles with high separation efficiency and purity. Therefore, in this system, the isolations of the 10 µM WBCs and 20 µm CTCs were performed in the trapezoidal CEA microchannel by varying the number of expansions in a fixed channel length. A high level of separation efficiency (>90%) was obtained for CTCs with more than 9 expansion numbers. Figure 12 depicts that the best performance of the microchannel (100% efficiency and 95% purity) is achieved for the CTCs by 10 expansion numbers, which provide a 10-mm microchannel length that is 1/3 of the microchannel used by Al-Halhouli (27) to focus the 10 µm and 5 µm particles.
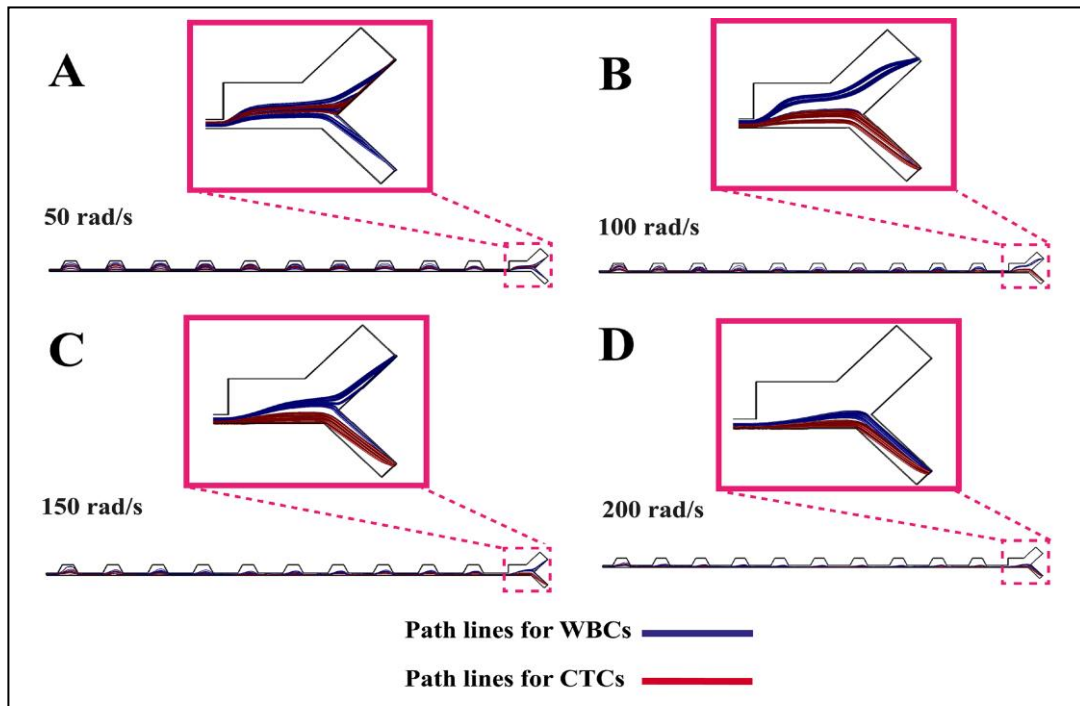


**Figure 11**. Path lines of the CTCs and WBCs in the separation microchannel and their position at the outlets at different angular velocities; A) 50 rad/s , B) 100 rad/s, C) 150 rad/s, and D) 200 rad/s.
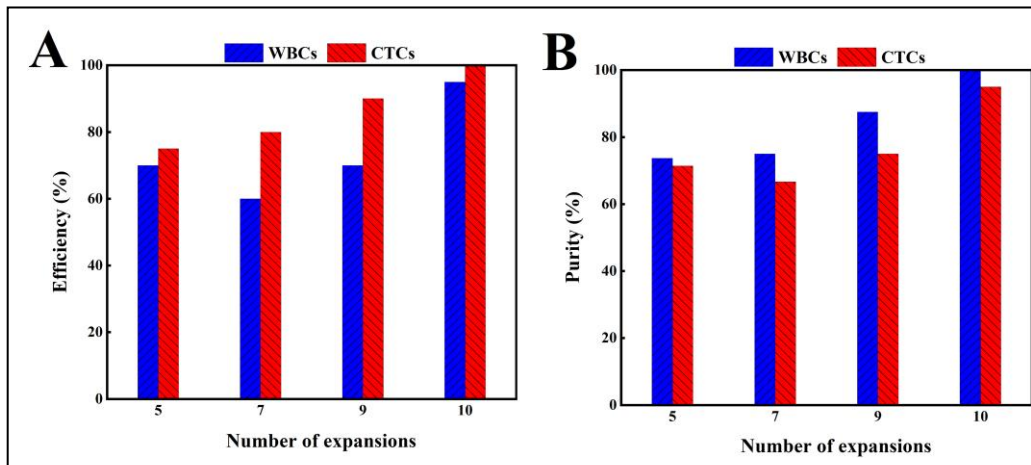
**Figure 12**. Separation performance versus expansion number: A) Efficiency, B) Purity

### 3.4.4. Dean Vortex Formation by Contraction Zone Aspect Ratio

As noticed in the prior sections, the magnitudes and directions of the migration across streamlines are determined by balancing between $F_L$ and $F_D$ applied to the particles. $F_D$, which is produced by the Dean Vortices, is formed at a certain distance from the microchannel contraction region. The height of the microchannel cross-section directly affects the quality of the Dean Vortices and velocity. Therefore, it changes the particles' equilibrium position by changing the flow velocity and magnitude of the forces applied to the cells. Simulations are performed for different microchannel depths from 80 µm To 140 µm with a 20 µm increment to find the optimal value. Figure 13 illustrates the Dean vortices for these different contraction heights. An increase in the contraction aspect ratio (h/w) boosts the fluid flow velocity and improves the Dean vortices. Improved vortex leads particles to experience various forces based on their size; nonetheless, increasing the channel height affects the maximum shear stress applied on the particles. By considering 100 µm for the microchannel height, the maximum radial velocity in the microchannel is 0.5 m/s with the fully developed profile, producing the maximum shear stress of 10 Pa.

### 3.5. Separation Results with Considering the RBCs

To indicate the ability of the proposed platform for CTC separation from whole blood contents, RBCs with an 8 µm diameter are considered. In this regard, simulations were performed to separate the CTCs with 20 µm particle sizes from WBCs and RBCs with 14 µm and 8 µm particle sizes, respectively. A total of 120 particles, including 40 CTCs, 40 WBCs, and 40 RBCs with mentioned diameters, were suspended in the fluid. As can be seen in figure 14, CTCs with 20 µm particle sizes were collected in outlet 2 (lower outlet), while WBCs and RBCs with different sizes were directed into outlet 1 (upper outlet). Red lines represent the CTCs, whereas green and blue ones show the WBC and RBC path lines. Simulation results indicated 100% separation efficiency and 88% purity for CTCs.
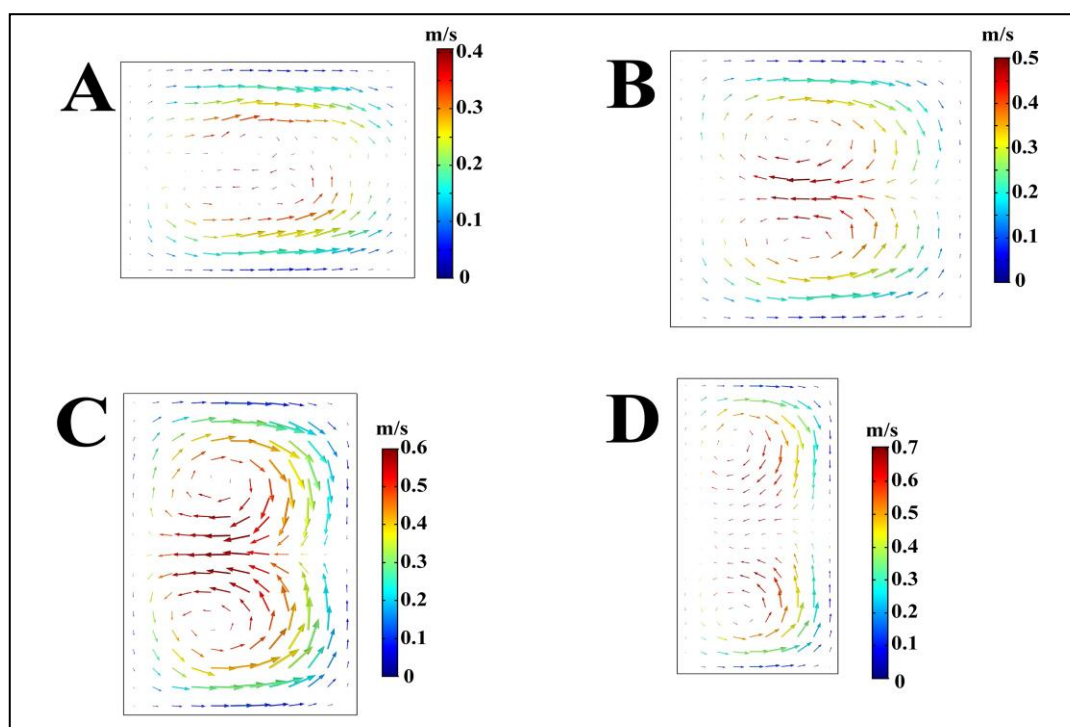
**Figure 13**. (A-D) Vortices at a distance of 30 µm from the contraction of the trapezoidal microchannel at different depths; A) 80 µm, B) 100 µm, C) 120 µm and D) 140 µm.
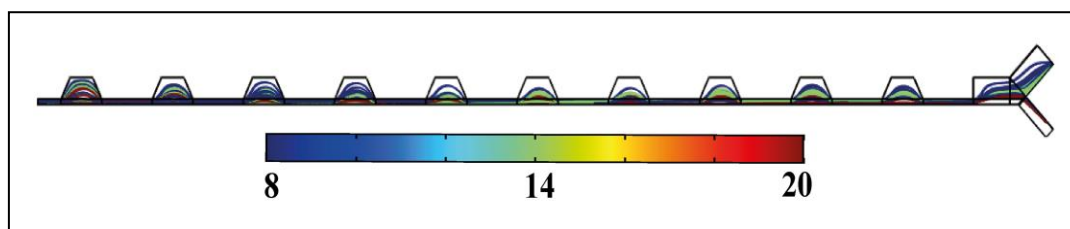


**Figure 14**. Path lines for 20 µm CTCs (red), 14 µm WBCs (green), and 8 µm RBCs (blue)

## 5. Conclusion

In this study, cells were considered to be rigid with a spherical shape; however, under different forces, they could be deformed and not be complete spheres. Additionally, to simplify the simulations, the number of cells was considered to be equal, which the quantity ratio between CTC and blood cells is normally over 10,000 times. As explained in section 4, in experimental works, due to the incubation of samples, the particle-particle interactions are not considered, which may provide changes in the achieved yields. These obtained simulation results can be used as a guide for future experimental works.

The separation and detection of CTCs have an essential role in cancer treatment. In this study, size-based CTC separation was examined in an LOD system. Inertial lift force, Dean Drag force, and centrifugal forces were considered to change the equilibrium positions of the CTCs and WBCs. Four expansion shapes (i.e., trapezoidal, circular, triangular, and rectangular) were simulated to obtain optimum microchannel geometry. Trapezoidal CEA microchannel represented high separation performance at a low angular velocity, compared to other micro-channels. The main results of this study are summarized as follows:

1. After an investigation of particle separation in the trapezoidal microchannel at four different depths of 80, 100, 120, and 140 µm, it was observed that by increasing the height of the contraction region, Dean Vortex formation improved. Nevertheless, it should be noted that the improvement in Dean Vortices will also increase forces and shear stress that affect the particles.

2. As the disk's rotational velocity increased, several separation patterns were observed at different fluid flow velocities. At low angular velocities, since the radial velocity was low and the inertial effects were not enough, the particles were not separated. However, over the optimum velocity, particles were focused and directed toward a specific outlet.

3. At the best condition, with the maximum radial velocity of 0.5 m/s across the 100-µm channel height, the system achieved 100% separation efficiency and 95% purity for the CTCs, while the maximum shear stress of 10 Pa affected the particles.

4. For whole blood, concerning the average diameter of 8 µm for RBCs, separation was possible with the same efficiency without the need for preparing samples or using the focusing fluid.

Finally, as the main result, these simulations can be used as a guide for future experimental works.

## Authors' Contribution

Study concept and design: M. T.

Acquisition of data: Sh. E.

Analysis and interpretation of data: Sh. E.

Drafting of the manuscript: M. T.

Critical revision of the manuscript for important intellectual content: M. T.

Statistical analysis: Sh. E.

Administrative, technical, and material support: M. T.

## Conflict of Interest

The authors declare that they have no known competing financial interests or personal relationships that could have appeared to influence the work reported in this paper.

## References

1. Farahinia A, Zhang WJ, Badea I. Novel microfluidic approaches to circulating tumor cell separation and sorting of blood cells: A review. J Sci-Adv Mater Dev. 2021;6(3):303-20.

2. Rostami P, Kashaninejad N, Moshksayan K, Saidi MS, Firoozabadi B, Nguyen N-T. Novel approaches in cancer management with circulating tumor cell clusters. J Sci-Adv Mater Dev. 2019;4(1):1-18.

3. Herath S, Razavi Bazaz S, Monkman J, Ebrahimi Warkiani M, Richard D, O'Byrne K, et al. Circulating tumor cell clusters: Insights into tumour dissemination and metastasis. Expert Rev Mol Diagn. 2020;20(11):1139-47

4. Lei KF. A review on microdevices for isolating circulating tumor cells. Micromachines. 2020;11(5):531.

5. Tahmasebipour M, Vafaie A. A novel single axis capacitive MEMS accelerometer with double-sided suspension beams fabricated using µWEDM. Sens Actuator A Phys. 2020;309:112003.

6. Tahmasebipour M, Modarres M, Salarpoor H, editors. Size Effect on the Deflection and Resonant Frequency of the Timoshenko Microbeam. 5th International Conference on Electrical and Computer Engineering; 2018.

7. Paknahad AA, Tahmasebipour M. An electromagnetic micro-actuator with PDMS-Fe3O4 nanocomposite magnetic membrane. Microelectron Eng. 2019;216:111031.

8. Tahmasebipour M, Paknahad AA. Unidirectional and bidirectional valveless electromagnetic micropump with PDMS-Fe3O4 nanocomposite magnetic membrane. J Micromech Microeng.. 2019;29(7):075014.

9. Tahmasebipour M, Modarres M, Salarpour H, editors. Investigation of Natural Frequency of Epoxy Micro-cantilevers via Finite Element Method and couple stress classical and strain gradient elasticity theories. 5th International Conference on Electrical and Computer Engineering; 2018.

10. Yue W-Q, Tan Z, Li X-P, Liu F-F, Wang C. Micro/nanofluidic technologies for efficient isolation and detection of circulating tumor cells. TrAC - Trends Anal. Chem. 2019;117:101-15.

11. Hao S-J, Wan Y, Xia Y-Q, Zou X, Zheng S-Y. Size-based separation methods of circulating tumor cells. Adv Drug Deliv Rev. 2018;125:3-20.

12. Dalili A, Samiei E, Hoorfar M. A review of sorting, separation and isolation of cells and microbeads for

biomedical applications: Microfluidic approaches. Analyst. 2019;144(1):87-113.

13.    Bayareh M. An updated review on particle separation in passive microfluidic devices. Chem Eng Process: Process Intensif. 2020;153:107984.

14.    Warkiani ME, Khoo BL, Wu L, Tay AKP, Bhagat AAS, Han J, et al. Ultra-fast, label-free isolation of circulating tumor cells from blood using spiral microfluidics. Nat Protoc. 2016;11(1):134-48.

15.    Guan G, Wu L, Bhagat AA, Li Z, Chen PC, Chao S, et al. Spiral microchannel with rectangular and trapezoidal cross-sections for size based particle separation. Sci Rep. 2013;3(1):1-9.

16.    Shiriny A, Bayareh M. Inertial focusing of CTCs in a novel spiral microchannel. Chem Eng Sci. 2021;229:116102.

17.    Lee A, Park J, Lim M, Sunkara V, Kim SY, Kim GH, et al. All-in-one centrifugal microfluidic device for size-selective circulating tumor cell isolation with high purity. Anal Chem. 2014;86(22):11349-56.

18.    Che J, Yu V, Dhar M, Renier C, Matsumoto M, Heirich K, et al. Classification of large circulating tumor cells isolated with ultra-high throughput microfluidic Vortex technology. Oncotarget. 2016;7(11):12748.

19.    Zhang J, Guo Q, Liu M, Yang J. A lab-on-CD prototype for high-speed blood separation. J Micromech Microeng. 2008;18(12):125025.

20.    Kuo J-N, Chen X-F. Decanting and mixing of supernatant human blood plasma on centrifugal microfluidic platform. Microsyst Technol. 2016;22(4):861-9.

21.    Park J-M, Kim MS, Moon H-S, Yoo CE, Park D, Kim YJ, et al. Fully automated circulating tumor cell isolation platform with large-volume capacity based on lab-on-a-disc. Anal Chem. 2014;86(8):3735-42.

22.    La M, Park SJ, Kim HW, Park JJ, Ahn KT, Ryew SM, et al. A centrifugal force-based serpentine micromixer (CSM) on a plastic lab-on-a-disk for biochemical assays. Microfluidics and Nanofluidics. 2013;15(1):87-98.

23.    Morijiri T, Sunahiro S, Senaha M, Yamada M, Seki M. Sedimentation pinched-flow fractionation for size-and density-based particle sorting in microchannels. Microfluidics and nanofluidics. 2011;11(1):105-10.

24.    Maria K, Gerson RA, Vitaly E, Jens D, editors. Lab-on-a disc platform for particle focusing induced by inertial forces. ProcSPIE; 2013.

25.    Aguirre GR, Efremov V, Kitsara M, Ducree J. Integrated micromixer for incubation and separation of cancer cells on a centrifugal platform using inertial and dean forces. Microfluidic Nanofluidics. 2015;18(3):513-26.

26.    Shamloo A, Mashhadian A. Inertial particle focusing in serpentine channels on a centrifugal platform. Phys. Fluids. 2018;30(1):012002.

27.    Al-Halhouli Aa, Doofesh Z, Albagdady A, Dietzel A. High-efficiency small sample microparticle fractionation on a femtosecond laser-machined microfluidic disc. Micromachines. 2020;11(2):151.

28.    Nasiri R, Shamloo A, Akbari J, Tebon P, R Dokmeci M, Ahadian S. Design and simulation of an integrated centrifugal microfluidic device for CTCs separation and cell lysis. Micromachines. 2020;11(7):699.

29.    Tahmasebipour M, Vafaie A. A highly sensitive three axis piezoelectric microaccelerometer for high bandwidth applications. Micro and Nanosystems. 2017;9(2):111-20.

30.    Mirzaaghaian A, Ramiar A, Ranjbar AA, Warkiani ME. Application of level-set method in simulation of normal and cancer cells deformability within a microfluidic device. J Biomech. 2020;112:110066.

31.    Madadelahi M, Acosta-Soto LF, Hosseini S, Martinez-Chapa SO, Madou MJ. Mathematical modeling and computational analysis of centrifugal microfluidic platforms: A review. Lab Chip. 2020;20(8):1318-57.

32.    Carlo DD, Irimia D, Tompkins RG, Toner M. Continuous inertial focusing, ordering, and separation of particles in microchannels. 2007;104(48):18892-7.

33.    Lee MG, Shin JH, Bae CY, Choi S, Park J-K. Label-free cancer cell separation from human whole blood using inertial microfluidics at low shear stress. Anal Chem. 2013;85(13):6213-8.

34.    Ying Y, Lin Y. Inertial focusing and Separation of particles in Similar curved channels. Sci Rep. 2019;9(1):1-12.

35.    Zhou J, Kulasinghe A, Bogseth A, O'Byrne K, Punyadeera C, Papautsky I. Isolation of circulating tumor cells in non-small-cell-lung-cancer patients using a multi-flow microfluidic channel. Microsyst Nanoeng. 2019;5(1):1-12.

36.    Dhar M, Pao E, Renier C, Go DE, Che J, Montoya R, et al. Label-free enumeration, collection and downstream cytological and cytogenetic analysis of circulating tumor cells. Sci Rep. 2016;6(1):1-12.